

Simple method for determining asymptotic states of fast neutrino-flavor conversion

Masamichi Zaizen^{1,*} and Hiroki Nagakura²

¹*Faculty of Science and Engineering, Waseda University, Tokyo 169-8555, Japan*

²*Division of Science, National Astronomical Observatory of Japan, 2-21-1 Osawa, Mitaka, Tokyo 181-8588, Japan*

(Dated: November 18, 2022)

Neutrino-neutrino forward scatterings potentially induce collective neutrino oscillation in dense neutrino gases in astrophysical sites such as core-collapse supernovae (CCSN) and binary neutron star mergers (BNSM). In this paper, we present a detailed study of fast neutrino-flavor conversion (FFC), paying special attention to asymptotic states, by linear stability analysis and local simulations with a periodic boundary condition. We find that asymptotic states can be characterized by two key properties of FFC: (1) the conservation of lepton number for each flavor of neutrinos and (2) the disappearance of ELN(electron neutrino-lepton number)-XLN(heavy-leptonic one) angular crossings in the spatial- or time-averaged distributions. The system which initially has the positive (negative) ELN-XLN density reaches a flavor equipartition in the negative (positive) ELN-XLN angular directions, and the other part compensates it to preserve the conservation laws. These properties of FFCs offer an approximate scheme determining the survival probability of neutrinos in asymptotic states without solving quantum kinetic equations. We also demonstrate that the total amount of flavor conversion can vary with species-dependent neutrino distributions for identical ELN-XLN ones. Our results suggest that even shallow or narrow ELN angular crossings have the ability to drive large flavor conversion, exhibiting the need for including the effects of FFCs in the modeling of CCSN and BNSM.

I. INTRODUCTION

A copious amount of neutrinos are emitted from inner regions of core-collapse supernovae (CCSN) and binary neutron star mergers (BNSM). Their inner dynamics are sensitive to neutrino physics, including neutrino-matter interactions, energy/momentum/lepton transport, and flavor conversion. Quantifying the impact of each element is one of the major tasks in developing theoretical models of CCSNe and BNSM.

Neutrinos can change their flavors during the propagation, which may affect fluid dynamics and nucleosynthesis in CCSNe and BNSM through neutrino-matter interactions. In environments with dense neutrino media, refractive effects by neutrino self-interactions play non-negligible roles in flavor conversions or even become dominant in the neutrino oscillation Hamiltonian. This potentially leads to collective neutrino oscillation [1–7]. The oscillation frequency increases with the neutrino number density, and the wavelength can be much shorter than the scale height of the stellar structure. In the last two decades, slow instability (or slow flavor conversion), which occurs by interacting between vacuum and self-interaction potentials, has been studied and exhibited dramatic flavor conversions [8–11]. The slow flavor conversion is, however, suppressed by dense background matter due to the relatively slow oscillation scale [12–14]. It suggests that the flavor conversion does not occur in the vicinity of neutrino spheres, and the impact on CCSN and BNSM seems subtle. Although removing assumptions of symmetries, which have been commonly

imposed in the traditional approach, alleviates the suppression, recent numerical simulations suggest that the matter suppression is still dominant in the inner region of CCSN and BNSM [15–21].

Recently, fast neutrino-flavor conversion (FFC) has received significant attention. It evolves independently from vacuum potential, and the flavor conversion is purely dictated by self-interaction potentials. The time scale of the fast instability can be much shorter than the slow one, and therefore the large flavor conversion may happen even inside neutrino spheres [22–28]. The necessary and sufficient condition for the occurrence of FFC is equivalent to the presence of angular crossings with respect to $(f_{\nu_\alpha} - f_{\bar{\nu}_\alpha}) - (f_{\nu_\beta} - f_{\bar{\nu}_\beta})$ [29, 30] (hereafter called ELN-XLN angular crossings), where f_{ν_α} and $f_{\bar{\nu}_\alpha}$ denote the distribution function of α -type flavor neutrinos and their anti-partners, respectively. In the context of CCSN and BNSM, the three-species treatment (ν_e , $\bar{\nu}_e$, and ν_X), corresponding to the condition that heavy-leptonic flavors have identical distributions, is a reasonable approximation (but see Refs. [31, 32]). As a result, the stability condition can be essentially reduced to the presence of crossings in the electron-neutrino lepton number (ELN) angular distribution (see, e.g., Refs. [33–37]). This motivated ELN crossing searches in neutrino data of recent simulations. These studies indicate that FFC likely occurs in CCSN [38–48] and in BNSM [49–53]. This exhibits the importance of studying the non-linear regime of FFC.

Studying flavor evolution in the non-linear phase requires directly solving a quantum kinetic equation (QKE). At the moment, global simulations of QKE are far from achieved due to computational limitations, and therefore recent efforts for FFC have focused on local simulations [54–68]. They demonstrated that the fast insta-

* zaizen@heap.phys.waseda.ac.jp

bility propagates in space, developing coherent structures of flavor conversion and interference with nearby components. In the non-linear phase, small-scale structures of flavor conversion emerge stochastically similar to turbulent cascades, eventually reaching an asymptotic state (or quasi-steady state) with sustaining large-scale asymmetric structures. Although there has been significant progress in developing numerical simulations, our physical understanding of the non-linear dynamics of FFC is still limited. Some key questions remain unanswered; what ingredients characterize the quasi-steady state (see also Refs. [60, 62, 67])?; how neutrino-matter interactions (collision term) alter dynamics of flavor conversions (see also Refs. [69–77])?; is there any qualitative difference in the quasi-steady state between local- and global scales (see also [78, 79])? Answering these questions requires a complementary analysis shining the spotlight on key quantities characterizing the non-linear dynamics of flavor conversion.

In this paper, we explore detailed features of asymptotic states of FFC by means of linear stability analysis and local simulations with a periodic boundary condition. This study also provides the rationale for the results of our previous works; flavor conversions reach a quasi-steady state in which ELN-XLN angular crossings disappear [78, 79]; how the boundary condition of the simulation box has an influence on the asymptotic state [80], which is associated with a conservation law of ELN and XLN. Based on these arguments, we provide an approximate scheme to determine the asymptotic states of FFC for a periodic boundary condition, which is in reasonable agreement with numerical simulations¹.

The paper is organized as follows. We describe two requirements determining the final fates of local FFC in terms of the stability analysis and the conservation laws in Sec. II. We then present how FFC eliminates the angular crossings and establishes a quasi-steady state in Sec. III. Finally, we conclude and discuss our study in Sec. IV.

II. CHARACTERIZATION OF FLAVOR EVOLUTION

We can obtain the flavor evolution by directly calculating the non-linear QKE for the neutrino self-interactions. At first, we will analyze what characterizes the behaviors of FFC before performing the non-linear simulation.

¹ In our previous paper [79], we provide the same approximate scheme but for the Dirichlet boundary condition.

A. Stability analysis for asymptotic state

Neutrino flavor conversions can be described by a QKE for density matrices of neutrinos:

$$(\partial_t + \mathbf{v} \cdot \nabla)\rho = -i[\mathcal{H}, \rho] + \mathcal{C}. \quad (1)$$

Here we consider the plane-parallel geometry to drop the advection term of neutrino angular directions in the momentum space. The Hamiltonian \mathcal{H} of neutrino oscillations is

$$\mathcal{H} = U \frac{M^2}{2E} U^\dagger + v^\mu \Lambda_\mu + \sqrt{2} G_F \int d\Gamma' v^\mu v'_\mu \rho', \quad (2)$$

where Γ specifies the neutrino energy E and the flight direction \mathbf{v} . Following the same convention as Ref. [81], the phase-space integration is $\int d\Gamma = \int_{-\infty}^{+\infty} dE E^2 \int d\mathbf{v} / (2\pi)^3$. In the first term, M^2 and U denote the mass-squared matrix and the Pontecorvo-Maki-Nakagawa-Sakata matrix, respectively. The second term represents matter-induced oscillation, where $v^\mu = (1, \mathbf{v})$ and $\Lambda_\mu = \sqrt{2} G_F \text{diag}[\{j_\mu^\ell\}]$. In the study, we ignore the collision term for simplicity.

For an effective two-flavor scenario, we can decompose the density matrix at a certain space-time position (t, \mathbf{x}) into the trace- and traceless parts as,

$$\rho(t, \mathbf{x}) = \frac{\text{Tr}\rho}{2} \mathbb{1}_2 + \frac{f_{\nu_e} - f_{\nu_x}}{2} \begin{pmatrix} s & S \\ S^* & -s \end{pmatrix}, \quad (3)$$

where s is a real number, S is a complex one, and f_{ν_α} is an occupation number density for a flavor α . We note that time dependence of the traceless part (the second term in the right-hand side of Eq. (3)) is handled by s and S in our method, indicating that the prefactor $((f_{\nu_e} - f_{\nu_x})/2)$ can be determined arbitrarily. In this study, we adopt spatial-averaged distributions at the beginning of each simulation ($t = 0$). On the other hand, all time- and spatial dependence in the trace part (the first term in the right-hand side of Eq. (3)) is handled by $\text{Tr}\rho$ (which does not affect flavor conversion, though). We define a spatial-averaged spectral difference between ν_e and ν_x at $t = 0$ as

$$g_{E,\mathbf{v}} = \begin{cases} f_{\nu_e} - f_{\nu_x} & \text{for } E > 0 \\ f_{\bar{\nu}_x} - f_{\bar{\nu}_e} & \text{for } E < 0 \end{cases}. \quad (4)$$

By using these variables, the governing equation for S (the off-diagonal component of the traceless part) can be written as,

$$\begin{aligned} i v^\mu \partial_\mu S_{E,\mathbf{v}} &= -\omega_V \cos 2\theta_V S_{E,\mathbf{v}} - \omega_V \sin 2\theta_V s_{E,\mathbf{v}} \\ &+ v^\mu (\Lambda_\mu^{11} - \Lambda_\mu^{22}) S_{E,\mathbf{v}} \\ &+ S_{E,\mathbf{v}} v^\mu \int d\Gamma' v'_\mu g_{E',\mathbf{v}'} s_{E',\mathbf{v}'} \\ &- s_{E,\mathbf{v}} v^\mu \int d\Gamma' v'_\mu g_{E',\mathbf{v}'} S_{E',\mathbf{v}'}, \end{aligned} \quad (5)$$

while

$$\begin{aligned} iv^\mu \partial_\mu s_{E,\mathbf{v}} &= \frac{\omega_V}{2} \sin 2\theta_V (S_{E,\mathbf{v}}^* - S_{E,\mathbf{v}}) \\ &+ \frac{1}{2} S_{E,\mathbf{v}}^* v^\mu \int d\Gamma' v'_\mu g_{E',\mathbf{v}'} S_{E',\mathbf{v}'} \\ &- \frac{1}{2} S_{E,\mathbf{v}} v^\mu \int d\Gamma' v'_\mu g_{E',\mathbf{v}'} S_{E',\mathbf{v}'}^* \end{aligned} \quad (6)$$

is the equation for s (the diagonal component). In the expression, ω_V and θ_V denote a vacuum frequency and a mixing angle, respectively. It should be stressed that any approximations are not imposed in deriving Eqs. (5) and (6) from QKE.

Below, let us prepare the stability analysis in the non-linear phase. In the linear regime (under the choice of fixed points as flavor eigenstates), the diagonal term is given by $s = \sqrt{1 - |S|^2} \simeq 1$, which can be directly inserted to Eq. (5), and then we can obtain the dispersion relation for S with the plane wave ansatz. In the non-linear regime, however, s would substantially deviate from unity, and more importantly, it depends on time and space, which causes mode couplings (in other words, we need to compute the convolutions of S with s). It should also be mentioned that the stability needs to be determined globally, if the background component is not uniform. These are main obstacles to deriving dispersion relation for S in the non-linear regime.

In our prescription, we drop the mode coupling by assuming that s is constant (but not unity). One may choose s as that at (t, \mathbf{x}) , i.e., the space-time location where the stability analysis is conducted. Another prescription is to adopt the spacial- or time-averaged quantity. In fact, we are interested in the overall trend of non-linear saturation and quasi-steady state of flavor conversion, which can be characterized by those averaged distributions. In the following, we leave the notation as s , but need to keep in mind this assumption.

We adopt the plane wave ansatz to S ,

$$S_{E,\mathbf{v}}(t, \mathbf{x}) \propto Q_{E,\mathbf{v}}(\Omega, \mathbf{K}) e^{-i(\Omega t - \mathbf{K} \cdot \mathbf{x})}, \quad (7)$$

and then the governing equation for $S_{E,\mathbf{v}}$ can be recast into

$$v^\mu k_\mu Q_{E,\mathbf{v}} = -\omega_V Q_{E,\mathbf{v}} - s_{E,\mathbf{v}} v^\mu \int d\Gamma' v'_\mu g_{E',\mathbf{v}'} Q_{E',\mathbf{v}'}, \quad (8)$$

where $k_\mu \equiv (\omega, \mathbf{k}) = K_\mu - \Lambda_\mu^{ex} - \Phi_\mu^{ex}$ with $\Lambda_\mu^{ex} \equiv \Lambda^{11} - \Lambda^{22}$ and $\Phi_\mu^{ex} = \int d\Gamma v_\mu g_{E,\mathbf{v}} s_{E,\mathbf{v}}$. In a co-rotating frame where the vacuum term oscillates quickly and the off-diagonal terms are averaged to zero by the matter term, the mixing angle θ_V can be set to zero. As a result, the nontrivial solutions for $Q_{E,\mathbf{v}}$ are given by, using the metric $\eta = \text{diag}(+, -, -, -)$,

$$D(\omega, \mathbf{k}) \equiv \det [\Pi^{\mu\nu}(k)] = 0, \quad (9)$$

where

$$\Pi^{\mu\nu} = \eta^{\mu\nu} + \int d\Gamma g_{E,\mathbf{v}} s_{E,\mathbf{v}} \frac{v^\mu v^\nu}{v^\lambda k_\lambda + \omega_V}. \quad (10)$$

We note that ω_V dependence accounts for the slow flavor conversion. It may be useful to rewrite Eq. (10) as

$$\Pi^{\mu\nu} = \eta^{\mu\nu} + \int d\Gamma g_{E,\mathbf{v}}^{ex}(t, \mathbf{x}) \frac{v^\mu v^\nu}{v^\lambda k_\lambda + \omega_V}, \quad (11)$$

where

$$\begin{aligned} g_{E,\mathbf{v}}^{ex}(t, \mathbf{x}) &= (P_{ee} g_{E,\mathbf{v}}^e + P_{xe} g_{E,\mathbf{v}}^x) - (P_{ex} g_{E,\mathbf{v}}^e + P_{xx} g_{E,\mathbf{v}}^x) \\ &= (P_{ee} - P_{ex}) g_{E,\mathbf{v}} \\ &= g_{E,\mathbf{v}} s_{E,\mathbf{v}}(t, \mathbf{x}). \end{aligned} \quad (12)$$

In the expression, we use the relation of $P_{ex} = (1 - s_{E,\mathbf{v}})/2$, where $P_{\alpha\beta}$ is defined as a transition probability from α -type flavor at the initial state to β -type one at t . If there is a nonzero imaginary part in k_μ , the flavor instability $S_{E,\mathbf{v}}$ can grow or dump in space and time.

FFC can be driven only by the neutrino self-interactions, and we can ignore the vacuum term. In the fast limit, $\omega_V = 0$, the density matrix loses the explicit energy-dependence in the QKE, and therefore Eq. (11) can be more concisely rewritten. We define an α -flavor lepton number (α LN) angular distribution

$$G_{\mathbf{v}}^\alpha = \sqrt{2} G_F \int_0^\infty \frac{dE E^2}{2\pi^2} [f_{\nu_\alpha}(E, \mathbf{v}) - f_{\bar{\nu}_\alpha}(E, \mathbf{v})] \quad (13)$$

and the difference $G_{\mathbf{v}}^{\alpha\beta} \equiv G_{\mathbf{v}}^\alpha - G_{\mathbf{v}}^\beta$ between α and β flavors. The dispersion relation only for fast instability is reduced to

$$D(\omega, \mathbf{k}) \equiv \det [\Pi^{\mu\nu}(k)] = 0, \quad (14)$$

where

$$\Pi^{\mu\nu} = \eta^{\mu\nu} + \int \frac{d\mathbf{v}}{4\pi} G_{\mathbf{v}}^{ex}(t, \mathbf{x}) \frac{v^\mu v^\nu}{v^\lambda k_\lambda}. \quad (15)$$

For the stability with respect to the spatial- or time-averaged distributions, we use the averaged quantity of $G_{\mathbf{v}}^{ex}(t, \mathbf{x})$ in Eq. (15).

A few remarks should be made here. The dispersion relation is essentially the same as that used in linear stability analysis. In fact, the growth (or damp) of S is determined solely by the diagonal components of the density matrix. Based on the same argument made by Ref. [29], the stability can be determined by the presence of ELN-XLN crossings even in the non-linear phase², suggesting that ELN-XLN angular distributions are fundamental quantities to characterize the dynamics of flavor

² However, a homogeneous mode can be stable even if there exists ELN-XLN crossing. This is simply because unstable solutions possibly appear only in inhomogeneous modes. Nevertheless, ELN-XLN angular distributions are key quantities to characterize the stability of FFC.

conversion. On the other hand, our method ignores the mode couplings with the inhomogeneity of ELN-XLN angular distributions. We will validate this condition by numerical simulations (see Sec. III).

B. Conservation laws

In the fast limit, the QKE can be decomposed into commutators with the neutrino density H_E and the flux H_F as

$$\begin{aligned} i(\partial_t + v_z \partial_z) \rho_v &= [H_{\nu\nu}, \rho_v] \\ &= [H_E, \rho_v] - [v_z H_F, \rho_v], \end{aligned} \quad (16)$$

where

$$H_E = \sqrt{2} G_F \int d\Gamma' \rho_{\nu'} \quad (17)$$

$$H_F = \sqrt{2} G_F \int d\Gamma' v'_z \rho_{\nu'}. \quad (18)$$

Moreover, integrating the QKE over the phase space, we can obtain

$$\partial_t H_E + \partial_z H_F = 0, \quad (19)$$

which has a conservative form without source terms. Note that the neutrino density is not locally conserved due to the advection (flux) term. Both ELN and XLN are conserved in terms of spatially integrated quantity because the neutrino flux on the boundary surface is closed in the periodic case. Therefore, flavor conversion proceeds with satisfying the ELN and XLN conservation and eventually reaches a non-linear saturation. In other words, FFC transfers the number density from the positive (negative) part to the negative (positive) and saturates when the angular distributions are wholly positive (negative) or zero. These properties offer a simple analytic prescription to determine an asymptotic state of FFC, which will be discussed in the next subsection.

Here, let us make an important remark. The spatial-integrated H_E is, in general, not conserved if another boundary condition is imposed. This implies that the system evolves towards a different asymptotic state; in fact we observed that the system settled into a qualitatively different quasi-steady state for the Dirichlet boundary condition, see Refs. [79, 80].

C. Asymptotic states

From the above discussion, we can predict the asymptotic states from two requirements: the disappearance of ELN-XLN angular crossings and the conservation of ELN and XLN. The disappearance of ELN-XLN angular crossings is equivalent to the achievement of flavor equipartition in some angular regions, which is determined as

follows³. If the total number density, $\int dv (\text{ELN} - \text{XLN})$, is positive, flavor conversion proceeds until the achievement of flavor equipartition on the angular parts with negative lepton number. In the other angular part, the ELN and XLN are adjusted so as to satisfy the number conservation of ELN and XLN. If the total number density is negative, flavor equipartition is achieved on the positive part, and then the conservation of ELN and XLN is adjusted in the negative one. Note that if the total number density of ELN-XLN is zero, complete flavor equipartition is established in the entire angular distribution, which is consistent with the result in [62].

Following the above consideration, we develop an approximate scheme. The negative ELN-XLN part A and positive one B are defined as

$$A \equiv \left| \int_{G_v^{ex} < 0} \frac{d\mathbf{v}}{4\pi} G_v^{ex} \right| \quad (20)$$

$$B \equiv \left| \int_{G_v^{ex} > 0} \frac{d\mathbf{v}}{4\pi} G_v^{ex} \right|. \quad (21)$$

When the total number density of ELN-XLN is positive, $B - A > 0$, the number density corresponding to $A/2$ is transferred from the ELN to the XLN in the negative ELN-XLN directions to establish a flavor equipartition. On the other hand, the same amount of number density is converted from the positive ELN-XLN parts to sustain the conservation for ELN (and XLN). Consequently, in the positive part, the number density $A/2$ is subtracted from the positive number density B and distributed into the XLN. Thereby, the survival probability of electron-type neutrinos can be analytically estimated as the following simple box-like formulas:

$$P_{ee} = \begin{cases} p & \text{for } G_v < 0 \\ 1 - (1-p) \frac{A}{B} & \text{for } G_v > 0 \end{cases}, \quad (22)$$

where p is a survival probability in the negative ELN-XLN part and becomes $p = p_{\text{eq}}$, where p_{eq} represents the survival probability for flavor equipartition, to eliminate the ELN-XLN crossing. Note that p_{eq} is 1/2 for two-flavor of neutrinos (see below for the case with a three-flavor framework). For the negative case, $B - A < 0$, considering the opposite, we obtain

$$P_{ee} = \begin{cases} p & \text{for } G_v > 0 \\ 1 - (1-p) \frac{B}{A} & \text{for } G_v < 0 \end{cases}. \quad (23)$$

In the symmetric flavor case $A = B$, our analytical scheme provides full flavor equipartition in the entire angular directions. Note that within a three-flavor framework, we need to consider flavor equipartitions on both

³ In this study, we assume that there is a single ELN-XLN crossing in initial angular profiles. The study of multiple ELN crossings is currently underway and will be reported in a forthcoming paper.

ELN-MuLN and ELN-TauLN simultaneously if they possess crossings. In the case that MuLN is identical to TauLN, which is a reasonable condition in CCSNe and BNSM, we set the flavor equilibrium point to $p_{\text{eq}} = 1/3$. One-half of the transition probability of electron-type neutrinos is transferred to each heavy-leptonic flavor as $P_{e\mu}$ and $P_{e\tau}$.

There is a caveat in the approximate scheme, however. The box-like structure in angular distributions of p would not be realistic. In fact, we will show in Sec. III that p does not change discontinuously at the crossing point but rather has a smooth profile. Nevertheless, the overall trend in asymptotic states of FFCs can be captured by the simple structure, and we leave its improvement to future work.

III. NUMERICAL TESTS

We perform numerical simulations on a periodic boundary condition, which validates our approach to determine asymptotic states of FFC. We assume a one-dimensional simulation box with axial-symmetry around the z -axis. As an initial state, we use the following ELN angular distribution, employed as G_{4b} in Ref. [59],

$$G_v^e = \mu [g_{\nu_e}(v) - \alpha g_{\bar{\nu}_e}(v)], \quad (24)$$

where $\mu = \sqrt{2}G_F n_{\nu_e}$, $\alpha = 0.92$ is an asymmetry parameter, and normalized angular distribution g_ν is defined as

$$g_\nu \propto \exp[-(v-1)^2/2\xi_\nu^2] \quad (25)$$

with $\xi_{\nu_e} = 0.6$ and $\xi_{\bar{\nu}_e} = 0.53$. We also assume that XLN is initially zero. Then, the ELN(-XLN) angular crossing is located at $v_c = 0.68$ and the ELN(-XLN) number density, $1 - \alpha$, is positive. Hence, we can predict that FFC proceeds so as to fill in the negative lepton number on more forward-directional side $v \gtrsim v_c$ relative to the angular crossing from the above requirements.

Figure 1 shows the dispersion relation $\Omega(K)$ satisfying Eq. (14) for the ELN angular distribution G_{4b} . Spatial modes K with nonzero imaginary parts $\text{Im}\Omega$ correspond to unstable branches and can induce FFC in the non-linear regime. In the bottom panel, we present the normalized eigenvector $|Q_v|$ with the maximum growth rate in the top panel and the peak amplitude is within the negative ELN directions, $v_z > v_c$. Consequently, the initial perturbation on the flavor coherent S evolves strongly within the crossing in the linear regime, and then flavor conversion can occur mainly in the angular directions in a non-linear phase. This picture agrees with the above prediction for the non-linear saturation. The behaviors of FFC in the non-linear regime will be demonstrated in Sec. III C.

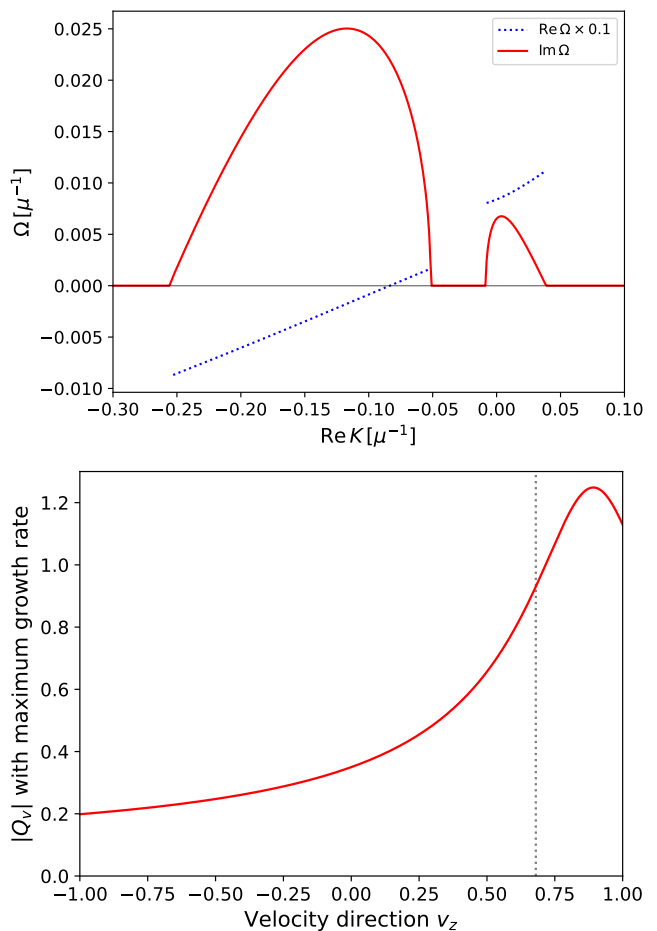


FIG. 1. Top: Dispersion relation of $\Omega(K)$ including unstable fast modes for ELN angular distribution G_{4b} . Solid (dotted) lines are for imaginary (real) parts of Ω . Bottom: Normalized amplitude $|Q_v|$ with a maximum growth rate in the top panel. Vertical dotted line is a crossing point, and we find that the peak is located within the negative ELN directions.

A. Setups

In the fast limit, neutrino density matrices lose the explicit energy-dependence in the QKE. Hence, antineutrinos are identified to those for neutrinos, i.e., $\bar{\rho}_\nu = \rho_\nu$. And we adopt a pseudo-spectral method using Fast Fourier Transformation implemented in the FFTW3 library⁴ to handle the spatial advection operator in the QKE (see Refs. [63, 66] on the detail and recent applications). Then, QKE for the spatial Fourier components in the polarization vector configuration $\rho \propto \mathbf{P} \cdot \boldsymbol{\sigma}$ is recast

⁴ Fastest Fourier Transform in the West, <http://www.fftw.org>.

into

$$\partial_t \tilde{\mathbf{P}}_v^K = -ivK \tilde{\mathbf{P}}_v^K + \sum_{K'} \left[\int dv' (1 - vv') G_{vv'}^e \tilde{\mathbf{P}}_{v'}^{K-K'} \times \tilde{\mathbf{P}}_v^{K'} \right]. \quad (26)$$

This equation includes the non-linear coupling term among all spatial modes K derived from the neutrino self-interactions. We initially put artificial spatially-inhomogeneous perturbations on the off-diagonal components of the density matrix to trigger flavor conversion instead of nonzero vacuum mixing. The spatial perturbation is

$$P_1(t=0, z, v_z) = \epsilon(z) \quad (27)$$

$$P_3(t=0, z, v_z) = \sqrt{1 - \epsilon(z)^2}, \quad (28)$$

where $\epsilon(z)$ is randomly arranged between 0 and 10^{-6} . The third component P_3 corresponds to the diagonal part of the density matrix and the decrease from unity implies the occurrence of a flavor transformation. In performing the flavor evolution in Eq. (26), once the initial conditions are built on the configuration space, they are converted into the Fourier space.

The self-interaction strength μ is a unique dimensional quantity in the QKE on the fast limit. Hence, we can measure the time and space with the unit of μ^{-1} . Then, we adopt a one-dimensional simulation box of $L_z = 1000$ spanned by a uniform grid $N_z = 10000$ with the periodic boundary condition. And we set 256 angular bins on the root of Legendre polynomials and use the Gauss-Legendre quadrature for the angular integration. We evolve Eq. (26) using the fourth-order Runge-Kutta scheme with a fixed time step size of $\Delta t = C_{\text{CFL}} \Delta z$, where the Courant-Friedrichs-Lewy number $C_{\text{CFL}} = 0.4$ as in Ref. [62].

B. ELN-XLN analysis

We perform the inhomogeneous modeling of local FFC with periodic boundary. In the fast limit, flavor conversion is determined only by the ELN-XLN angular distributions. Here, we focus on the time evolution of FFC in terms of ELN and XLN.

Figure 2 shows $P_3(t, z, v_z)$ on the space-velocity ($z - v_z$) plane at five representative time snapshots $t = 750, 1000, 2000, 3000,$ and 5000 . Flavor conversions emerge everywhere in space but mainly in $v_z \gtrsim 0.7$ for the angular direction. Once the flavor conversion enters into a non-linear phase, flavor waves interfere with each other mainly due to the spatial advection and then cultivate smaller-scale structures. After $t = 2000$, the entire system establishes a quasi-steady state with temporal and spatial variations.

To capture the overall trend of the quasi-steady state, we adopt the spatial-averaged $G_v^{ex}(t, \mathbf{x})$ in computing the dispersion relation. As we have already mentioned, the

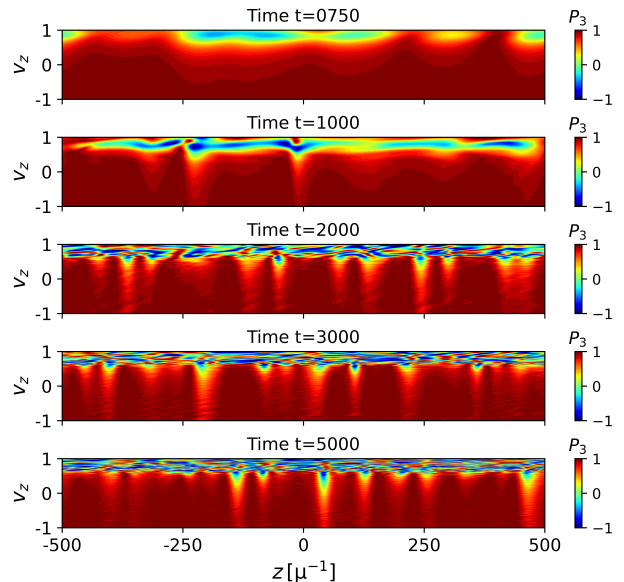


FIG. 2. $P_3(t, z, v_z)$ on the space-velocity ($z - v_z$) plane at five time snapshots $t = 750, 1000, 2000, 3000,$ and 5000 .

stability can be determined by the ELN-XLN angular crossing; hence, we focus on ELN-XLN distributions below. Figure 3 portrays spatial-averaged flavor coherent $\langle S \rangle$ and ELN-XLN distributions as a function of time and neutrino angle in the top and middle panels, meanwhile we also display some relevant quantities of angular distribution at $t = 5000$ in the bottom one. As shown in the top panel, the spatial-averaged flavor coherent $\langle S \rangle$ is clearly small even for the late phases and is $\lesssim 0.1$, and then the neutrino density matrix is almost in the flavor state. As shown in the middle panel, the ELN-XLN in $v_z \gtrsim 0.7$ approaches to zero with time (transiting from blue to white), meanwhile it has a subtle change in other angular directions. In the early phase when flavor conversion starts to occur, large-scale coherent oscillation appears, but it cascades to small scale with decreasing the amplitude. This indicates that the system establishes a quasi-steady state. Assuming that s is constant in the quasi-steady state based on the two panels, the stability of FFC can be evaluated through the spatially-averaged ELN-XLN angular distributions. We can delve into the detailed angular distributions in the quasi-steady state, at $t = 5000$, in the bottom panel of Fig. 3. As shown in the panel, the ELN angular distribution still has a crossing even after the non-linear saturation. However, XLN is no longer zero due to flavor conversion, and we find that it compensates the angular distribution so as to make ELN-XLN be zero in $v_z \gtrsim 0.7$. This is the reason why further flavor conversion does not occur in the spatially averaged domain in our simulation, which is consistent with our claim obtained by the stability analysis. As a result, the spatial-averaged ELN-XLN angular distribution is entirely positive or zero, and does not have any

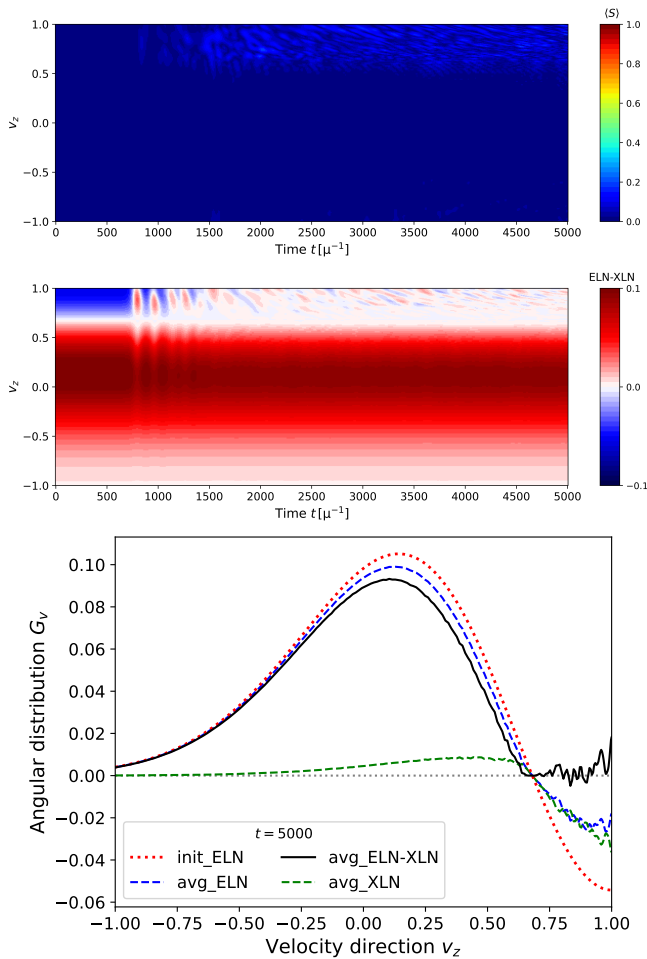


FIG. 3. Top: Spatial-averaged flavor coherent $\langle S \rangle$ on the $t - v_z$ plane. Middle: Spatial-averaged ELN-XLN angular distributions on the $t - v_z$ plane. Bottom: Spatial-averaged angular distributions for some important quantities at $t = 5000$. In the bottom panel, red dotted line is an initial ELN angular distribution. Blue (green) dashed line is an ELN (XLN) one. Black solid line corresponds to an ELN-XLN angular distribution, which exhibits that the angular crossing almost disappears.

crossings in all directions.

It may be interesting to compare non averaged- and time-averaged angular distributions, which are displayed in Fig. 4 as a function of z and v_z . The top panel portrays the ELN-XLN angular distributions at $t = 5000$, and the bottom one shows the time-averaged distributions during the time interval of $2000 \leq t \leq 5000$. As shown in the top panel, local ELN-XLN angular crossings remain even after the system settled into a quasi-steady state. This is attributed to large fluctuations in space with small-scale structures, in particular, at the angular region of $v_z \gtrsim 0.7$. On the other hand, the time-averaged ELN-XLN angular distributions smear out such local fluctuations and lead to a similar result as spatial-averaged distributions. Indeed, the ELN-XLN becomes

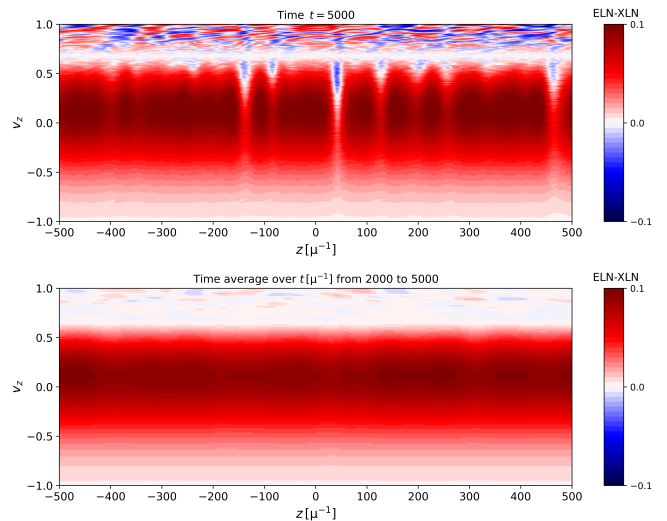


FIG. 4. Top panel: ELN-XLN distributions as a function of z and v_z at the end of the simulation ($t = 5000$). Bottom panel: same as the top panel but we take the average over time in the range of $2000 \leq t \leq 5000$. As shown in these panels, ELN-XLN angular crossings remain at $t = 5000$, whereas the crossings in time-averaged distributions become much less prominent.

almost zero in $v_z \gtrsim 0.7$, illustrating the disappearance of ELN-XLN angular crossing. This is consistent with our previous study [78, 79]. Our results suggest that FFC evolves toward eliminating the angular crossings in the ELN-XLN distribution, and the system establishes a quasi-steady state with saturating flavor conversion when the crossings disappear.

Finally, we apply our approximate scheme Eq. (22) to obtain spatial-averaged survival probability after a non-linear saturation. Figure 5 compares the numerical results to our analytical scheme. In the top panel, our model only broadly captures its characteristics, particularly around the crossing, because we disregard the detailed angular distributions for simplicity. Meanwhile, we find that despite such a rough model, our approximate ELN angular distribution reproduces the numerical one well. This is because the contribution from the compensation for the flavor equipartition is relatively small in the positive ELN parts. This is also because the ELN is close to zero near the crossing where the deviation from numerical simulations is the greatest. Consequently, our proposed scheme is very concise and in reasonable agreement with numerical simulations.

C. Species analysis

In the previous section, we have discussed the final fate of FFC in terms of ELN and XLN. In the fast limit, the asymptotic behaviors are determined only by the ELN-XLN angular distribution. On the other hand, the de-

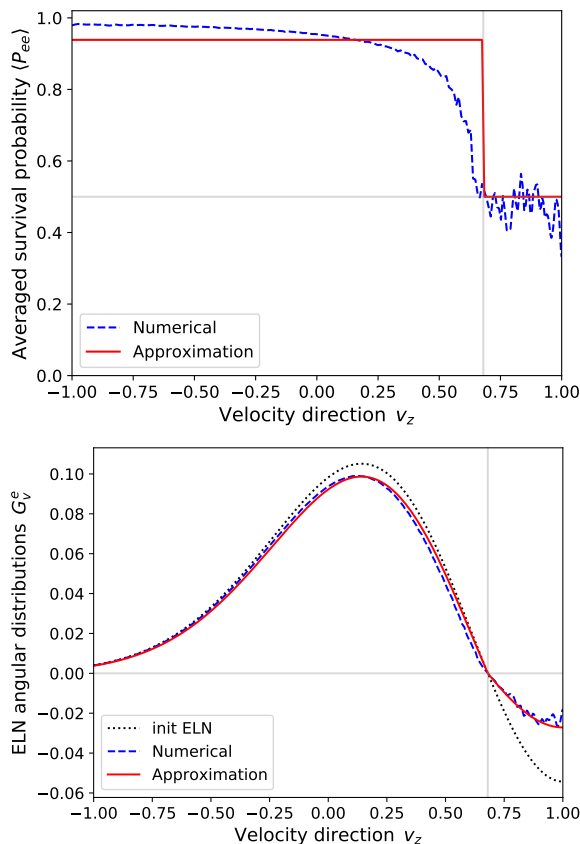


FIG. 5. Top: Spatial-averaged survival probability at $t = 5000$. Blue dashed line is for numerical simulation and red solid one is for our analytical scheme in Eq. (22). Horizontal thin line corresponds to a flavor equipartition $P_{ee} = 0.5$ and vertical one to the directions of an angular crossing. Bottom: ELN angular distributions averaged over space at $t = 5000$. Black dotted (blue dashed) lines are initial (final) ELN angular distributions and red solid one is from our analytical scheme in Eq. (22).

descriptions only give quantities about the difference between neutrinos and antineutrinos, not the number density or the mixing degree for each species. In the context of CCSNe and BNSMs, the number densities for ν_e and $\bar{\nu}_e$ are crucial to incorporate the feedback to neutrino transport, and the species-dependent neutrino angular distributions must be considered.

Here, we discuss angular-averaged flavor conversion on each neutrino species by using the angular distributions g_{ν_α} in Eq. (25), not the ELN angular distributions G_ν^e . Solid lines in the bottom panel in Fig. 6 exhibit the time evolution of survival probabilities of electron (anti-)neutrinos averaged over space and neutrino angle. This illustrates that the system reaches a non-linear saturation around $t = 2000$ as seen in Fig. 2. It should be mentioned that the actual steady state is never achieved, exhibiting that FFC involves stochastic fluctuations similar to turbulence. Also, we find that the averaged survival probability for $\bar{\nu}_e$ is slightly smaller than that for

ν_e . The difference hinges on the species dependence of angular distributions. Since $\bar{\nu}_e$ exceeds ν_e in the angular regions where FFC establishes flavor equipartition, $\bar{\nu}_e$ is more converted into the heavy-leptonic flavors compared than ν_e consequently. It means that while ELN-XLN angular distributions are sufficient to determine the dynamics of FFC, investigating the mixing degree requires species-dependent information.

Also, we plot averaged survival probabilities for our analytical model in Eq. (22) by two dots on $t = 5000$ in the bottom panel in Fig. 6. Our approximate scheme exhibits relatively close but slightly larger values compared than numerical results. The deviation comes from rough estimation near the angular crossing as shown in Fig. 5. For species-dependent angular distributions, the crossing is near the forward peak, so our analytical model tends to underestimate the conversion degree. Meanwhile, in terms of the ELN, the deviations in the neutrino and antineutrino sectors cancel each other and are reduced to negligible. This comparison lends confidence to our approximate scheme.

To delve further into the understanding of the asymptotic state of FFC, we focus on the species dependence of flavor conversion. FFC uniquely determines the time evolution of ELN and XLN angular distributions in the fast limit. It implies that as long as ELN-XLN angular distribution is identical, neutrinos with different species-dependent ones should experience the same flavor conversions. Hence, we consider the extreme cases with the same ELN angular distributions as G_{4b} below.

For the original ELN angular distribution in Fig. 3, it is possible to treat the positive ELN part ($v_z \lesssim 0.7$) as carried only by ν_e and the negative ELN part ($v_z \gtrsim 0.7$) as carried only by $\bar{\nu}_e$; we call it Case 1. Also, we can create another model which is bulked out only inside the angular crossing in the species-dependent angular distributions g_ν of G_{4b} ; we call it Case 2. The top panel of Fig. 6 shows the angular distributions of ν_e and $\bar{\nu}_e$ for three cases. G_{4b} (solid), Case 1 (dashed), and Case 2 (dotted) all generate identical ELN angular distributions and induce the same FFC. On the other hand, since the fraction of number density distributed inside the angular crossing is distinct in each case, angle-averaged survival probability should exhibit different asymptotic values. In the bottom panel of Fig. 6, for Case 1, only $\bar{\nu}_e$ reaches the flavor equipartition within the angular crossing, and the conversion probability largely deviates that for ν_e . For Case 2, since the angular distributions are more forward-peaked, averaged survival probabilities are closer to the flavor equipartition $\langle P_{ee} \rangle = 0.5$ than for G_{4b} . We also plot averaged survival probabilities computed by our analytical model for both Case 1 (triangles) and Case 2 (stars) in the bottom panel. The errors to the result of numerical simulations are within a few percent for all cases (the greatest is $\sim 9\%$ for $\langle \bar{P}_{ee} \rangle$ in G_{4b}). This comparison clearly shows that our approximate scheme has the ability to capture species-dependent features.

Note that the angular distributions for Case 1 and Case

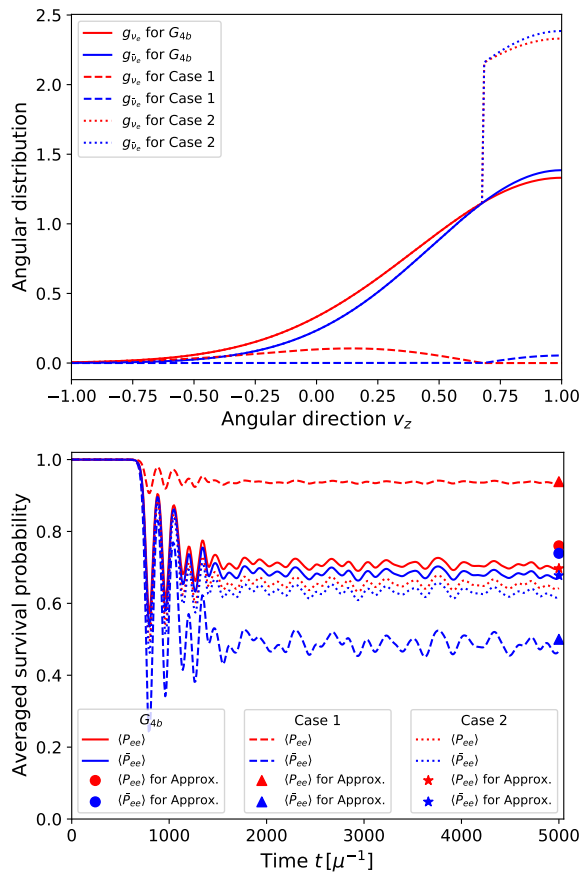


FIG. 6. Top: angular distributions of electron (anti-)neutrinos for three cases. Solid red- (blue-)colored lines are angular distributions for G_{Ab} . Dashed and dotted ones for Case 1 and Case 2, respectively. Each case generates the identical ELN angular distribution and induces the same FFC. Bottom: Time evolution of survival probabilities of electron (anti-)neutrino averaged over the spatial domain and the angular distributions $g_{\nu\alpha}$ for three cases. Quite different conversion probabilities are exhibited. Circle, triangle, and star markers at $t = 5000$ correspond to those estimated by our analytical scheme in Eq. (22) for each case.

2 are not normalized in Fig. 6. Thereby, even though the transition probability of $\bar{\nu}_e$ for Case 1 is the largest, the converted number density of $\bar{\nu}_e$ for Case 2 is the largest. Such behaviors imply that the depth and the width of ELN-XLN angular crossings are not directly involved in the averaged survival probability and the converted number density. Suppose the angular direction where the flavor equipartition is achieved covers the peak of angular distributions. In that case, electron-type neutrinos are well converted into heavy-leptonic flavors even if the angular crossing is shallow. Generically, angular crossings generated in realistic CCSNe are relatively shallow or narrow, though FFC possibly essentially alters the neutrino number density.

IV. CONCLUSIONS

In this paper, we have presented asymptotic states of fast neutrino-flavor conversion (FFC) in local simulations with a periodic boundary condition. Flavor instability exponentially grows by following the dispersion relation in the linear phase, and FFC occurs, gradually establishing a quasi-steady state. We have investigated what determines the non-linear saturation in terms of the stability analysis and the conservation law for electron neutrino-lepton number (ELN) and heavy one (XLN).

Our numerical simulations show that the system reaches a quasi-steady state when the averaged ELN-XLN angular distribution has no crossings. It is consistent with our stability analysis, suggesting that our proposed method is beneficial for analyzing the spatial- and time-averaged properties of flavor conversions. It is worth noting that ELN-XLN angular crossings exist instantaneously, indicating that the flavor conversion would not be saturated locally. It is also consistent with the results of our simulations, in which the exact steady state is not established, and small-scale modulations still occur within the crossing. Our stability analysis illustrates the importance of ELN-XLN angular distributions to characterize the dynamics of fast flavor conversion even in the non-linear phase, and we conclude that the system evolves toward eliminating the ELN-XLN angular crossings (not those of ELN).

Also, we have proposed an analytic scheme determining the survival probability of each neutrino species. Our approximate scheme is constructed to satisfy two requirements: the disappearance of ELN-XLN angular crossings (a flavor equipartition) and the conservation laws for ELN (XLN). We demonstrated that the overall trend of FFCs in asymptotic states can be qualitatively determined by the two conditions, and we provided the numerical recipe as an approximate scheme (see Eqs. (22) and (23)).

We have exhibited the averaged survival probabilities for angular distributions different in electron-type neutrinos but with identical ELN ones. ELN-XLN angular distributions characterize the dynamics of FFC and uniquely determine the quasi-steady state. On the other hand, the conversion degree for each species is mainly determined by how many neutrinos are distributed in the directions where a flavor conversion, particularly a flavor equipartition, is induced. Our results emphasize the importance of species-dependent information for the total amount of flavor conversion. Even if the angular crossings are shallow or narrow, they can significantly affect the flavor contents after the non-linear saturation.

Although our presented descriptions for the non-linear phase of FFC are very clear and it will be useful to develop the sub-grid model of FFC, there remain some crucial issues. As discussed in the present study, the boundary condition is a key ingredient to characterize the asymptotic state, but it is a non-trivial issue which boundary condition (periodic or Dirichlet) is appropriate.

This would hinge on both global and local properties of neutrino radiation fields and needs to be investigated in detail. It is interesting to note that the quasi-steady state with a periodic boundary condition temporarily appeared in the early phase of FFC simulations in our previous study [79], in which we employed the Dirichlet boundary condition. We witnessed that such a quasi-steady state is sustained up to the time when the neutrinos emitted from the inner boundary reach there, but it transits to another asymptotic state at the end of the simulation. This suggests that we need to consider the asymptotic state of FFC with arbitrary boundary conditions. We leave its detailed study to future work. Another crucial issue would be the impact of collisions; indeed, FFC could be qualitatively different due to the multi-energy effects of neutrino-matter interactions [72]. The asymptotic state of FFC with collisions would be considered by correcting Eq. (19) (adding the source term and restor-

ing the energy-dependence in QKE); the detailed study is also currently underway. As such, there are many works to be needed, but the study of the asymptotic state, as done in the present study, will shed light on key ingredients characterizing flavor conversion even in such complex systems.

ACKNOWLEDGMENTS

We are grateful to Shoichi Yamada and Tomoya Takiwaki for useful comments and discussions. MZ is supported by the Japan Society for Promotion of Science (JSPS) Grant-in-Aid for JSPS Fellows (Grants No. 22J00440) from the Ministry of Education, Culture, Sports, Science, and Technology (MEXT) in Japan. The numerical computations were carried out on Cray XC50 at the Center for Computational Astrophysics, National Astronomical Observatory of Japan.

-
- [1] J. Pantaleone, *Physics Letters B* **287**, 128 (1992).
 - [2] J. Pantaleone, *Physical Review D* **46**, 510 (1992).
 - [3] G. Sigl and G. Raffelt, *Nuclear Physics B* **406**, 423 (1993).
 - [4] H. Duan, G. M. Fuller, and Y.-Z. Qian, *Annual Review of Nuclear and Particle Science* **60**, 569 (2010).
 - [5] S. Chakraborty, R. Hansen, I. Izaguirre, and G. Raffelt, *Nuclear Physics B Neutrino Oscillations: Celebrating the Nobel Prize in Physics 2015*, **908**, 366 (2016).
 - [6] I. Tamborra and S. Shalgar, *Annual Review of Nuclear and Particle Science* (2021), 10.1146/annurev-nucl-102920-050505.
 - [7] S. Richers and M. Sen, (2022), arXiv:2207.03561 [astro-ph, physics:hep-ph].
 - [8] H. Duan, G. M. Fuller, J. Carlson, and Y.-Z. Qian, *Physical Review D* **74**, 105014 (2006).
 - [9] S. Hannestad, G. G. Raffelt, G. Sigl, and Y. Y. Y. Wong, *Physical Review D* **74**, 105010 (2006).
 - [10] G. Fogli, E. Lisi, A. Marrone, and A. Mirizzi, *Journal of Cosmology and Astroparticle Physics* **2007**, 010 (2007).
 - [11] B. Dasgupta, A. Dighe, G. G. Raffelt, and A. Y. Smirnov, *Physical Review Letters* **103**, 051105 (2009).
 - [12] A. Esteban-Pretel, A. Mirizzi, S. Pastor, R. Tomàs, G. G. Raffelt, P. D. Serpico, and G. Sigl, *Physical Review D* **78**, 085012 (2008).
 - [13] S. Chakraborty, T. Fischer, A. Mirizzi, N. Saviano, and R. Tomàs, *Physical Review Letters* **107**, 151101 (2011).
 - [14] S. Sarikas, I. Tamborra, G. Raffelt, L. Hüdepohl, and H.-T. Janka, *Physical Review D* **85**, 113007 (2012).
 - [15] G. Raffelt, S. Sarikas, and D. d. S. Seixas, *Physical Review Letters* **111**, 091101 (2013).
 - [16] S. Chakraborty, A. Mirizzi, N. Saviano, and D. d. S. Seixas, *Physical Review D* **89**, 093001 (2014).
 - [17] G. Mangano, A. Mirizzi, and N. Saviano, *Physical Review D* **89**, 073017 (2014).
 - [18] B. Dasgupta and A. Mirizzi, *Physical Review D* **92**, 125030 (2015).
 - [19] S. Chakraborty, R. S. Hansen, I. Izaguirre, and G. G. Raffelt, *Journal of Cosmology and Astroparticle Physics* **2016**, 028 (2016).
 - [20] F. Capozzi, B. Dasgupta, and A. Mirizzi, *Journal of Cosmology and Astroparticle Physics* **2016**, 043 (2016).
 - [21] M. Zaizen, S. Horiuchi, T. Takiwaki, K. Kotake, T. Yoshida, H. Umeda, and J. F. Cherry, *Physical Review D* **103**, 063008 (2021).
 - [22] R. F. Sawyer, *Physical Review D* **72**, 045003 (2005).
 - [23] R. F. Sawyer, *Physical Review D* **79**, 105003 (2009).
 - [24] R. F. Sawyer, *Physical Review Letters* **116**, 081101 (2016).
 - [25] S. Chakraborty, R. S. Hansen, I. Izaguirre, and G. G. Raffelt, *Journal of Cosmology and Astroparticle Physics* **2016**, 042 (2016).
 - [26] B. Dasgupta, A. Mirizzi, and M. Sen, *Journal of Cosmology and Astroparticle Physics* **2017**, 019 (2017).
 - [27] S. Shalgar and I. Tamborra, (2022), 10.48550/arXiv.2206.00676, arXiv:2206.00676 [astro-ph, physics:hep-ph].
 - [28] S. Shalgar and I. Tamborra, (2022), arXiv:2207.04058 [astro-ph, physics:hep-ph].
 - [29] T. Morinaga, *Physical Review D* **105**, L101301 (2022).
 - [30] B. Dasgupta, *Physical Review Letters* **128**, 081102 (2022).
 - [31] R. Bollig, H.-T. Janka, A. Lohs, G. Martínez-Pinedo, C. J. Horowitz, and T. Melson, *Physical Review Letters* **119**, 242702 (2017).
 - [32] T. Fischer, G. Guo, G. Martínez-Pinedo, M. Liebendörfer, and A. Mezzacappa, *Physical Review D* **102**, 123001 (2020).
 - [33] I. Izaguirre, G. Raffelt, and I. Tamborra, *Physical Review Letters* **118**, 021101 (2017).
 - [34] F. Capozzi, B. Dasgupta, E. Lisi, A. Marrone, and A. Mirizzi, *Physical Review D* **96**, 043016 (2017).
 - [35] C. Yi, L. Ma, J. D. Martin, and H. Duan, *Physical Review D* **99**, 063005 (2019).
 - [36] M. Delfan Azari, S. Yamada, T. Morinaga, W. Iwakami, H. Okawa, H. Nagakura, and K. Sumiyoshi, *Physical Review D* **99**, 103011 (2019).
 - [37] M. Chakraborty and S. Chakraborty, *Journal of Cosmol-*

- ogy and Astroparticle Physics **2020**, 005 (2020).
- [38] S. Abbar, H. Duan, K. Sumiyoshi, T. Takiwaki, and M. C. Volpe, *Physical Review D* **100**, 043004 (2019).
- [39] H. Nagakura, T. Morinaga, C. Kato, and S. Yamada, *The Astrophysical Journal* **886**, 139 (2019).
- [40] M. Delfan Azari, S. Yamada, T. Morinaga, H. Nagakura, S. Furusawa, A. Harada, H. Okawa, W. Iwakami, and K. Sumiyoshi, *Physical Review D* **101**, 023018 (2020).
- [41] S. Abbar, H. Duan, K. Sumiyoshi, T. Takiwaki, and M. C. Volpe, *Physical Review D* **101**, 043016 (2020).
- [42] T. Morinaga, H. Nagakura, C. Kato, and S. Yamada, *Physical Review Research* **2**, 012046 (2020).
- [43] R. Glas, H.-T. Janka, F. Capozzi, M. Sen, B. Dasgupta, A. Mirizzi, and G. Sigl, *Physical Review D* **101**, 063001 (2020).
- [44] S. Abbar, *Journal of Cosmology and Astroparticle Physics* **2020**, 027 (2020).
- [45] F. Capozzi, S. Abbar, R. Bollig, and H.-T. Janka, *Physical Review D* **103**, 063013 (2021).
- [46] H. Nagakura, A. Burrows, L. Johns, and G. M. Fuller, *Physical Review D* **104**, 083025 (2021).
- [47] A. Harada and H. Nagakura, *The Astrophysical Journal* **924**, 109 (2022).
- [48] R. Akaho, A. Harada, H. Nagakura, W. Iwakami, H. Okawa, S. Furusawa, H. Matsufuru, K. Sumiyoshi, and S. Yamada, (2022), 10.48550/arXiv.2206.01673, arXiv:2206.01673 [astro-ph].
- [49] M.-R. Wu and I. Tamborra, *Physical Review D* **95**, 103007 (2017).
- [50] X. Li and D. M. Siegel, *Physical Review Letters* **126**, 251101 (2021).
- [51] O. Just, S. Abbar, M.-R. Wu, I. Tamborra, H.-T. Janka, and F. Capozzi, *Physical Review D* **105**, 083024 (2022).
- [52] S. Richers, *Physical Review D* **106**, 083005 (2022).
- [53] E. Grohs, S. Richers, S. M. Couch, F. Foucart, J. P. Kneller, and G. C. McLaughlin, (2022), 10.48550/arXiv.2207.02214, arXiv:2207.02214 [astro-ph, physics:hep-ph, physics:nucl-th].
- [54] B. Dasgupta, A. Mirizzi, and M. Sen, *Physical Review D* **98**, 103001 (2018).
- [55] F. Capozzi, M. Chakraborty, S. Chakraborty, and M. Sen, *Physical Review Letters* **125**, 251801 (2020).
- [56] L. Johns, H. Nagakura, G. M. Fuller, and A. Burrows, *Physical Review D* **102**, 103017 (2020).
- [57] S. Shalgar and I. Tamborra, *Journal of Cosmology and Astroparticle Physics* **2021**, 014 (2021).
- [58] S. Shalgar and I. Tamborra, *Physical Review D* **104**, 023011 (2021).
- [59] J. D. Martin, C. Yi, and H. Duan, *Physics Letters B* **800**, 135088 (2020).
- [60] S. Bhattacharyya and B. Dasgupta, *Physical Review D* **102**, 063018 (2020).
- [61] S. Richers, D. E. Willcox, N. M. Ford, and A. Myers, *Physical Review D* **103**, 083013 (2021).
- [62] M.-R. Wu, M. George, C.-Y. Lin, and Z. Xiong, *Physical Review D* **104**, 103003 (2021).
- [63] M. Zaizen and T. Morinaga, *Physical Review D* **104**, 083035 (2021).
- [64] S. Richers, D. Willcox, and N. Ford, *Physical Review D* **104**, 103023 (2021).
- [65] S. Abbar and F. Capozzi, *Journal of Cosmology and Astroparticle Physics* **2022**, 051 (2022).
- [66] S. Richers, H. Duan, M.-R. Wu, S. Bhattacharyya, M. Zaizen, M. George, C.-Y. Lin, and Z. Xiong, *Physical Review D* **106**, 043011 (2022).
- [67] S. Bhattacharyya and B. Dasgupta, (2022), 10.48550/arXiv.2205.05129, arXiv:2205.05129 [astro-ph, physics:hep-ph].
- [68] F. Capozzi, M. Chakraborty, S. Chakraborty, and M. Sen, *Physical Review D* **106**, 083011 (2022).
- [69] S. Shalgar and I. Tamborra, *Physical Review D* **103**, 063002 (2021).
- [70] C. Kato, H. Nagakura, and T. Morinaga, *The Astrophysical Journal Supplement Series* **257**, 55 (2021).
- [71] H. Sasaki and T. Takiwaki, *Progress of Theoretical and Experimental Physics* **2022**, 073E01 (2022).
- [72] C. Kato and H. Nagakura, (2022), arXiv:2207.09496 [astro-ph].
- [73] J. D. Martin, J. Carlson, V. Cirigliano, and H. Duan, *Physical Review D* **103**, 063001 (2021).
- [74] G. Sigl, *Physical Review D* **105**, 043005 (2022).
- [75] L. Johns and H. Nagakura, *Physical Review D* **106**, 043031 (2022).
- [76] L. Johns and Z. Xiong, (2022), 10.48550/arXiv.2208.11059, arXiv:2208.11059 [astro-ph, physics:hep-ph].
- [77] Z. Xiong, M.-R. Wu, G. Martínez-Pinedo, T. Fischer, M. George, C.-Y. Lin, and L. Johns, (2022), 10.48550/arXiv.2210.08254, arXiv:2210.08254 [astro-ph, physics:hep-ph, physics:nucl-th].
- [78] H. Nagakura and M. Zaizen, (2022), arXiv:2206.04097 [astro-ph, physics:hep-ex, physics:hep-ph, physics:nucl-th].
- [79] H. Nagakura and M. Zaizen, (2022), 10.48550/arXiv.2211.01398, arXiv:2211.01398 [astro-ph, physics:hep-ex, physics:hep-ph, physics:nucl-th].
- [80] H. Nagakura, *Physical Review D* **106**, 063011 (2022).
- [81] S. Airen, F. Capozzi, S. Chakraborty, B. Dasgupta, G. Raffelt, and T. Stirner, *Journal of Cosmology and Astroparticle Physics* **2018**, 019 (2018).